A new technique for measuring the bed surface texture during flow and application to a degradational sand-gravel laboratory experiment

Orru, Clara; Blom, Astrid; Chavarrias Borras, Victor; Ferrara, V; Stecca, Guglielmo

DOI
10.1002/2016WR018938

Publication date
2016

Document Version
Final published version

Published in
Water Resources Research

AGU PUBLICATIONS

Water Resources Research

RESEARCH ARTICLE
10.1002/2016WR018938

Key Points:
- We present a technique for measuring the bed surface texture during flow in a flume run
- Sorting measurements provided new insights and enabled improved calibration of a numerical model
- A backwater due to partial transport led to a static armor governed by downstream fining

Correspondence to:
C. Orrú,
c.orru@tudelft.nl

Citation:
Orrú, C., A. Blom, V. Chavarrías, V. Ferrara, and G. Stecca (2016), A new technique for measuring the bed surface texture during flow and application to a degradational sand-gravel laboratory experiment, *Water Resour. Res.*, *52*, doi:10.1002/2016WR018938.

Received 21 MAR 2016
Accepted 29 AUG 2016
Accepted article online 1 SEP 2016

A new technique for measuring the bed surface texture during flow and application to a degradational sand-gravel laboratory experiment

Clara Orrú[1], Astrid Blom[1], Victor Chavarrías[1], Velia Ferrara[2], and Guglielmo Stecca[1,3,4]

[1]Faculty of Civil Engineering and Geosciences, Department of Hydraulic Engineering, Delft University of Technology, Delft, Netherlands, [2]Faculty of Engineering, Department of Environmental Engineering and Recovery, University of Naples Federico II, Naples, Italy, [3]National Institute of Water and Atmospheric Researc, Christchurch, New Zealand, [4]Department of Civil, Environmental and Mechanical Engineering, University of Trento, Italy

Abstract We present a new image analysis technique for measuring the grain size distribution (texture) of the bed surface during flow in a laboratory experiment. A camera and a floating device are connected to a carriage used to take images of the bed surface over the entire flume length. The image analysis technique, which is based on color segmentation, provides detailed data on spatial and temporal changes of the areal fraction content of each grain size at the bed surface. The technique was applied in a laboratory experiment conducted to examine a degradational reach composed of a well sorted two-fraction mixture of sand and gravel. The initial bed consisted of an upstream reach that was characterized by an imposed stepwise fining pattern (the bimodal reach) and a downstream sand reach. A lack of sediment supply and partial transport conditions led to the formation of a static armor in the bimodal reach, which resulted in a more abrupt spatial transition in the bed surface mean grain size. The associated spatial transition in slope led to a backwater effect over the bimodal reach, a streamwise reduction in sand mobility, and so a static armor that was governed by a downstream fining pattern. Although a morphodynamic equilibrium state under steady flow is generally characterized by normal flow, here the partial transport regime prevented the bed from adjusting toward normal flow conditions and the morphodynamic steady state was governed by a backwater. We applied a numerical morphodynamic sand-gravel model to reproduce the laboratory experiment. The numerical model captured the hydrodynamic and morphodynamic adjustment and the static armor well, yet the armoring occurred too slowly. Although the final configuration of the experiment shows features of a gravel-sand transition (i.e., a sudden transition in slope and mean grain size), we are hesitant to claim similarities between our results and the physical mechanisms governing a gravel-sand transition in the field.

1. Introduction

Techniques for measuring the grain size distribution of the bed surface during flow in a laboratory experiment are limited. *Suzuki and Michue* [1991] used a method in which they sampled sediment layers with a thickness of 5 mm using a spatula after stopping the flow. *Blom et al.* [2003] took core samples using a sampling box after draining the flume at different stages of a run. *Hassan and Church* [2000] took bed surface samples using a piston device without draining the flume. They reduced the flow rate to a level governed by no sediment transport. Such procedures are time consuming and destructive.

Recently image analysis has become more popular as it is a reliable, practical and nondestructive method. *Wilcock et al.* [2001] took images of a bed surface composed of colored particles after draining the flume. They positioned a grid over the images and registered the color of the grains at the grid intersections to determine the bed surface grain size distribution. Other authors applied particle counting techniques using images of the bed surface taken after draining the flume [*Mao et al.*, 2011; *Crowe Curran and Waters*, 2014] or images taken after decreasing the flow rate but without draining the flume [*Hassan et al.*, 2006]. *Piedra et al.* [2012] took four images (having a size of 460x610 mm) at 1 m intervals over the length of the flume during flow. Ultraviolet paint was used to recognize the coarser grains of the mixture using software that enables analysis of images taken under ultraviolet light. *Wu and Yang* [2004] determined the grain mobility

by taking photographs of the bed surface during a run over a 1.2 m long observation section. An acrylic floating plate was positioned on the water surface to reduce reflection and refraction. *Heays et al*. [2010a, 2010b, 2014] took images of a 1 m long section during an experiment to measure particle velocity and the bed surface texture. They added a V-shaped structure at the upstream end of a plexiglas plate to eliminate air bubbles. *Orrú et al*. [2014] combined image analysis, based on color segmentation, with a sediment removal technique to measure the bed surface texture and the size stratification of a sand-gravel deposit after draining the flume. For a more detailed review on the above image analysis techniques we refer to *Orrú et al*. [2014].

The first objective of this research is to develop and assess a new technique for measuring the grain size distribution of the bed surface during flow with transported sediment. The technique is an extension and an improvement of the one presented by *Orrú et al*. [2014]. The changes comprise: (a) an extension of the technique for measuring during flow and an automatic cropping of the images to cover the entire bed surface, (b) a new algorithm that allows for leaving one of the sediment fractions (sand) in its natural color to avoid cohesion-related issues, (c) the possibility to apply the new technique to sediment mixtures composed of up to 6 grain size fractions.

Our second objective is to study mixed sediment processes in a degradational laboratory experiment. Degradation generally results from (a) a temporal reduction or fining of the sediment supply from upstream, or (b) a temporal increase of the flow rate, or (c) a temporal decrease in base level. Under mixed-sediment conditions, bed degradation, for instance caused by a reduction of the sediment supply due to the presence of a dam, often leads to a coarsening of the bed surface [e.g., *Parker and Klingeman*, 1982; *Jain*, 1990]. Degradational problems have received little attention so far [e.g., *Galay*, 1983; *Gölz*, 1994]. Aggradational laboratory experiments were conducted to study the effects of sediment overloading using unisize sediment [*Bhamidipaty and Shen*, 1971; *Soni*, 1981; *Alves and Cardoso*, 1999] and mixed sediment [*Ribberink*, 1987; *Suzuki and Michue*, 1991; *Paola et al*., 1992; *Seal et al*., 1997; *Toro-Escobar et al*., 2000]. Examples of degradational studies using unisize sediment are the ones by *Newton* [1951] and *Bhamidipaty and Shen* [1971] and under mixed-size sediment conditions the ones by *Little and Mayer* [1972], *Yen et al*. [1992], *Hassan and Church* [2000], *Hassan et al*. [2006], and *Mao et al*. [2011]. Here we focus on degradational problems as they may be more complex than aggradational ones due to the interaction between surface and substrate sediment. Degradation of a mixed sediment bed usually leads to the exposure of substrate sediment but at the same time to a coarsening of the bed surface. This coarsening can prevent the entrainment of finer substrate sediment thus limiting or halting bed degradation. Further investigation on the interaction between these processes is needed. To this end we study the effects of a lack of sediment supply and partial transport on a laboratory sand-gravel reach.

Our third objective is to assess whether a numerical model system, based on the active layer model of *Hirano* [1971], can reproduce the laboratory experiment and to show how the image analysis technique can provide data that is useful in the calibration and validation of a numerical mixed sediment morphodynamic model. To this end, we apply a numerical sand-gravel model based on the Hirano equation and the backwater equation to the laboratory experiment.

2. New Technique for Measuring the Bed Surface Texture During Flow

2.1. Images of the Bed Surface During Flow

Our newly proposed technique for measuring the grain size distribution of the bed surface during flow builds on the technique proposed by *Orrú et al*. [2014]. The latter allows for measurement of the size stratification of a sand-gravel deposit after draining the flume. Here we extend the technique to enable measurement of the grain size distribution of the bed surface *during* a laboratory run over the entire flume length. Figure 1 shows the equipment used to take images of the bed surface. A camera was connected to a carriage, as well as a floating device made out of a glass plate and a wooden frame using PVC pipes. The bottom pipes had a smaller diameter than the upper ones to allow for vertical motion of the floating device and automatic adjustment of the level of the floating device to spatial changes in the water surface elevation. The floating device was slightly submerged, i.e., the glass plate was positioned more or less 1 cm below the water surface. It is therefore advised to use the equipment only when the ratio of the submerged depth ($\approx$ 1 cm) to the flow depth is sufficiently small to not significantly affect the flow. The width and length of the floating device were 0.38 m and 0.74 m, respectively. Following *Heays et al*. [2010a, 2010b] the

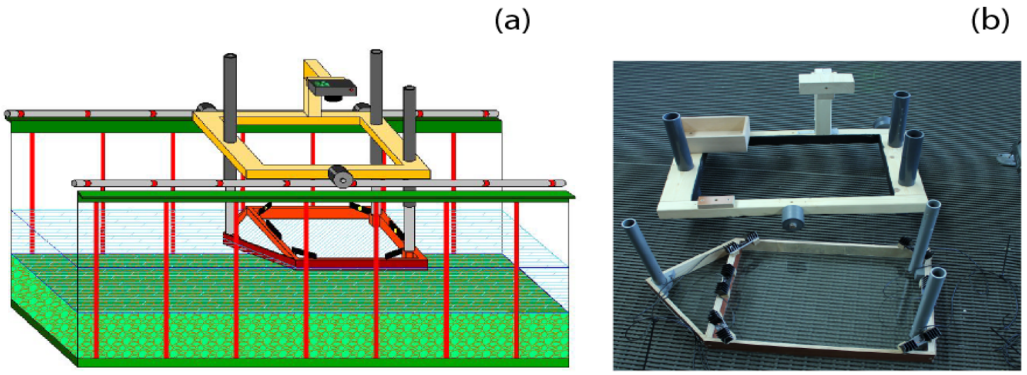

Figure 1. Equipment for measuring the grain size distribution of the bed surface during a laboratory experiment at flows with transported sediment: (a) sketch of how the equipment is used inside the flume; (b) image of the two parts of the equipment, the carriage and the floating device.

upstream part of the floating device was V-shaped to avoid air bubbles. Six small LED lights were mounted on the wooden frame of the floating device to illuminate the bed surface and avoid reflections. They were mounted on small cooling plates to prevent them from overheating.

2.2. Image Analysis

We process the images of the bed surface using a Matlab algorithm that provides the areal fraction content of a surface covered by a certain color. Each color corresponds to a certain grain size. The sediment mixture used in the experiment was composed of a sand fraction (D_{50}=1.05 mm) and a gravel fraction (D_{50}=14 mm). The gravel particles were painted green whereas the sand was unpainted to avoid cohesion-related issues. Here we extend and improve the image analysis algorithm presented by *Orrú et al*. [2014] to allow for measuring the bed surface texture during flow and to provide an automatic cropping of the images and an improved detection of the colors.

The robustness of the technique was assessed by *Orrú et al*. [2014]. They observed that the particle coloring had negligible effect on the grain size distribution. In other words, after sieve analysis little difference was found between the grain size distribution of the original and the painted sediment mixture. Also, they found that the particle coloring had negligible effect on the density of the sediment. Images of a submerged bed surface showed slightly better results regarding the measured grain size distribution than for a drained situation, and the flow depth did not affect the resulting measured grain size distribution. The results of the image analysis were successfully compared to the ones of sieve analysis, and the conversion model of *Parker* [1991a, 1991b] was applied to convert the areal fraction content resulting from image analysis into a volumetric fraction content.

The first step in the image analysis procedure consists of automatically cropping the images. To this end red stripes were positioned every 0.28 m in streamwise direction on each side wall of the flume (Figure 1a). Cropping then requires the coordinates of two positions (A′ and B) at opposite corners of the image (Figure 2). The color of the stripes is recognized using the Matlab code, which provides a segmented image consisting of the red pixels of the stripes only. In these images we find the two points located between the edge of the stripes and the bed (Figure 2c), which are used as cropping coordinates.

The color segmentation, which is the division of pixels into color groups, is performed in the Lab color space. The Lab color space is composed of three dimensions: the luminosity dimension L and the color (or chromatic) dimensions a and b. In the code we use a bi-dimensional space based on the coordinates a and b only (Figure 3). Depending on its color a pixel of an image has a certain location in the color space. Based on this location the pixel is assigned to a color group. Here the color segmentation is based on polygons rather than *Orrú et al*.'s [2014] method based on forced cluster centres, because the current polygon method provides a larger freedom and therefore shows improved color segmentation results. We use polygons to delimit areas of the Lab color space and the amount of pixels within each delimited area or polygon then provides the areal fraction content covered by a color and so grain size.

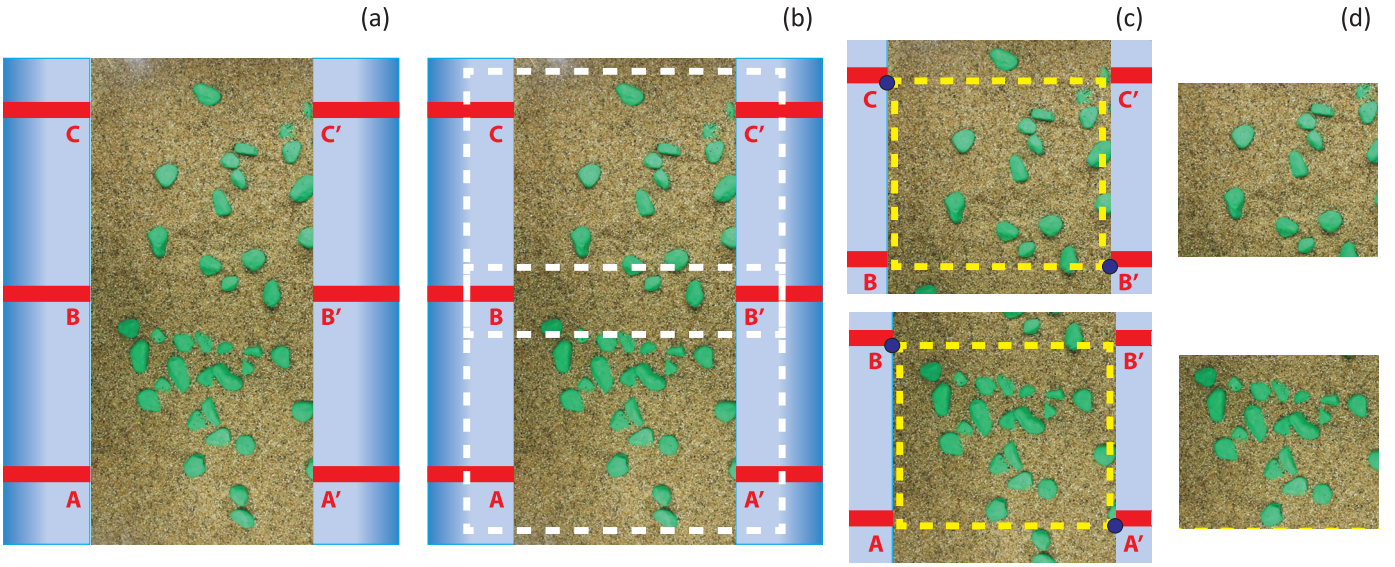

Figure 2. Method for automatically cropping the images and obtaining full coverage of the bed surface: (a) top view of the flume and red stripes fixed to the flume walls; (b) the white dashed lines showing two images taken with a certain overlap; (c) each image showing two red stripes on each side of the flume. Two points on opposite corners of the image (i.e., B and A′) are detected and its coordinates are used to crop the image (yellow dashed line); (d) resulting cropped images.

The preparatory part consists of the initial determination of the polygons, which needs to be done once for a certain color combination. If *N* colors are used, *N-1* polygons are defined. The polygons are determined analysing a limited number of images, i.e., the target images. These target images are created with an imposed grain size distribution combining *N* images of an equal number of pixels each of a unisize sediment and so single color group (Figure 3a). The images used to create the target image should be taken under the same conditions (light, submerged or unsubmerged) as the images to which the image analysis method will be applied. The procedure to determine the polygons is summarized as follows:

1. *Reading of target image*.
   We load the RGB target images with an imposed grain size distribution.
2. *Image conversion from RGB color space to Lab color space*.
   We convert the RGB values of each pixel into the Lab color space values.
3. *Definition of polygon boundaries*.
   The pixels of the target image (black dots) are plotted in the Lab color space to visually analyze their distribution (Figure 3b). Because of the two grain sizes considered here the pixel distribution shows two dominant modes in the color space: one mode covering a green sector and the other one an orange-yellow sector. Two straight lines from the centre of the circle to the edge (represented by boundaries 1 and 2 in Figure 3b) are used to initially subdivide the pixel sectors and thus the color space into *N* color groups. The initial position of the boundaries (red lines) is defined by the user after visual analysis of the pixel distribution in Figure 3b. Since the optimal polygons are determined by testing several possible solutions to the final position of the boundaries by an algorithm, as will be explained in point 4, it is necessary to define a certain 'width' over which the boundary is allowed to be moved (Figure 3b). Alternatively, the initial position of the boundaries and the width can be randomly generated by an algorithm, yet a definition by the user is preferred to allow for a faster computation.
4. *Generation of polygons*.
   Within the area set by the boundaries and the width, a certain number of flexible points (i.e., white points) is imposed at which the polygon is allowed to move between the dashed lines of Figure 3b. The position of each of these flexible points is varied using a Monte Carlo simulation to find the optimal polygon performance. In each simulation (a) different (set of) polygon(s) is used to segment the pixels into color groups and the amount of pixels in each color group provides data on the areal fraction content. The optimal (set of) polygon(s) is found when the values of the areal fraction content are closest to the ones of the target images, here resulting in the green polygon in Figure 3c.

   After this preparatory part the images of the bed surface are processed. The procedure to determine the areal fraction content of the grain sizes is summarized as follows:

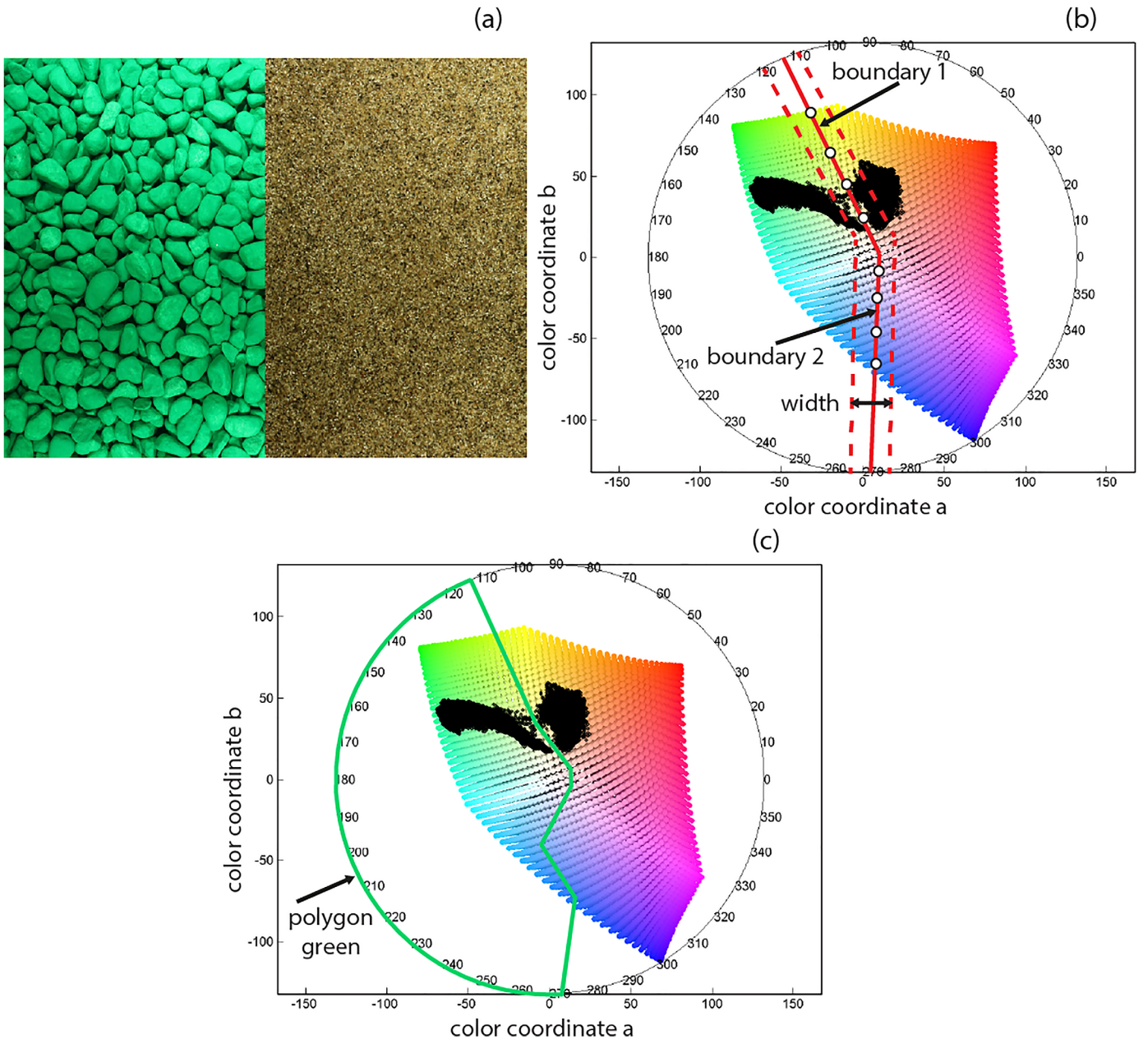

Figure 3. Illustration of the image analysis algorithm: (a) target image with an imposed areal fraction content (for each colour equal to 0.5) used to define the optimal polygon; (b) bi-dimensional view of the *a* and *b* domain of the Lab colour space and pixels of the target image (black dots). The operator sets the boundaries (red lines), a certain width (the shortest distance between the two red dashed lines), and a certain number of points (white dots) at which the boundary is moved; (c) the resulting polygon (green line) is used to segment the pixels into two color groups (green and natural color).

5. *Initialization of the polygon variables*.
   The coordinates of the polygon defined in steps 1–4 are set as input parameters.
6. *Reading of image*.
   We load the RGB images of the bed surface.
7. *Image conversion from RGB color space to Lab color space*.
   We convert the RGB values of each pixel into Lab color space values.
8. *Color segmentation using polygons*.
   We now divide the Lab color space into *N* areas using *N-1* polygons. The position of each pixel in the color space determines to which color group the pixel is assigned.

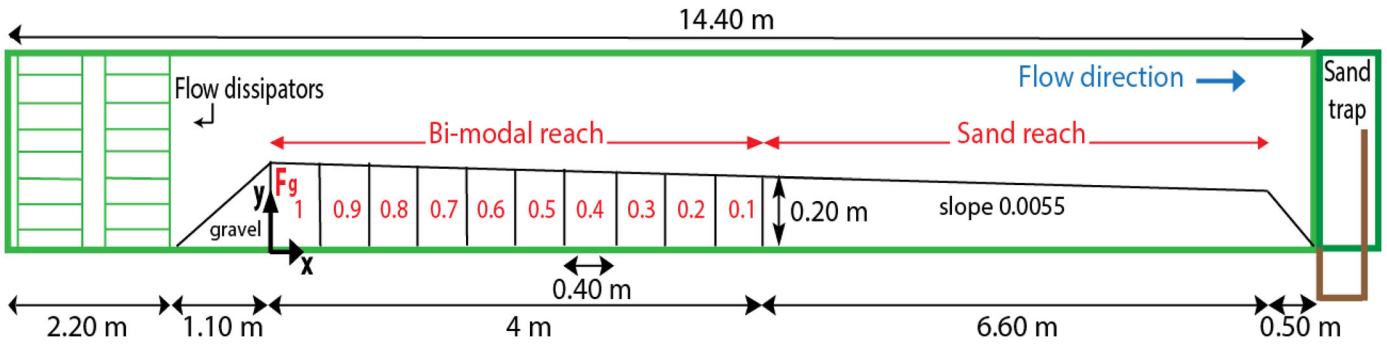

Figure 4. Flume set up, the initial bed and the coordinate system. The red numbers indicate the volumetric gravel fraction content in each compartment of the initial bed.

9. *Calculation of areal fraction content covered by each color*.
   The amount of pixels within each polygon enables computation of the areal fraction content covered by a color and therefore grain size.

The newly proposed algorithm shows better results than the *Orrú et al*. [2014] method as mostly shadow-rich grains show an improved color segmentation. Using the target images we now obtain a higher accuracy of the algorithm. Color combinations in which one of the grain sizes has a natural, usually variable, color (while the other fractions are painted) are now accurately segmented. This latter improvement enables us to avoid painting the sand fraction, which is beneficial as painted sand particles may behave in a cohesive manner. The algorithm can be applied to combinations composed of more than 2 colors. A combination of 6 colors (so 6 well sorted size fractions) was tested and successfully analyzed. If their natural color is relatively uniform and sufficiently different from each other, more than 1 grain size fraction can be used in its natural color. The new code has a slightly larger computational time than the one of *Orrú et al*. [2014].

3. Experimental Set-up

3.1. The Experimental Settings

We apply our new technique for measuring the grain size distribution of the bed surface to a degradational laboratory experiment. The experiment was conducted at the Water Laboratory of the Faculty of Civil Engineering and Geosciences of Delft University of Technology. The tilting flume was 14.40 m long, 0.40 m wide, and 0.45 m high. The water discharge was controlled by a water pump at the upstream end of the flume and the downstream water level was controlled by a tailgate at the downstream end of the flume. The sediment was caught in a sediment trap at the downstream end of the flume.

The initial bed was governed by a uniform slope (0.0055), an imposed stepwise fining pattern, and a downstream sand reach (Figure 4). The sand content in the initial bed increased in streamwise direction in steps of 10 percent for each compartment (bimodal reach) up to the location where the bed was fully composed of sand (sand reach) to study how limited sediment supply conditions affect a sand-gravel reach that is governed by an initial stepwise fining pattern. The bimodal reach was composed of 10 compartments, each one 0.40 m long and 0.20 m thick (Figure 4). Each compartment was created delimiting it using two metal sheets of 2 mm thickness. The sand was moistened with water and mixed with the gravel to obtain a homogeneous mixture within each compartment. Small volumes of about 1/6 of the total compartment volume were mixed and installed, which was repeated until each compartment was filled. Before the experiment was started the metal sheets delimiting the compartments were carefully removed.

No sediment was supplied from upstream. The water discharge was equal to 0.0368 m^3/s and maintained constant during the experiment. The downstream water surface elevation was decreased in two steps during the first 3 flow hours to gradually reach the required flow conditions and was then maintained constant for the remainder of the experiment (Figure 5). The total duration of the experiment was 25 h. The Froude number varied between 0.3 and 0.8 (subcritical flow) as flow conditions varied in space and time during the experiment.

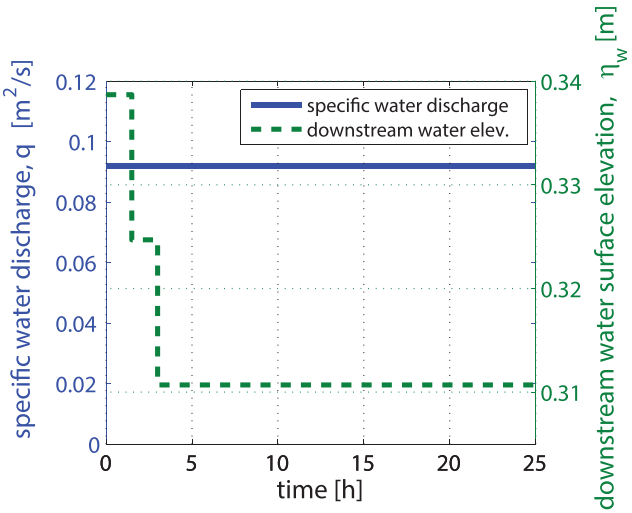

Figure 5. Water discharge per unit width, q, and base level, η_w, imposed in the laboratory experiment.

3.2. Measurements

The imposed water discharge was continuously measured using a flow meter positioned at the input water pipe based on the travel time of an acoustic signal. The downstream water level was continuously measured with a laser instrument at the downstream end of the flume (at x = 10.40 m). Longitudinal bed and water surface elevation profiles were measured every 30 min using two laser instruments mounted on a carriage. The laser instrument measuring bed elevation was positioned inside a watertight box that was slightly submerged to avoid reflections of the signal on the water surface. The box was eye-shaped to minimize disturbance of the flow. The sediment transport rate at the downstream end of the flume was measured by collecting and weighing the sediment caught in the sediment trap, after it was pumped to a small tank besides the flume. The flow rate was such that only the sand was mobile. Every hour the amount of sand in the tank was collected and later dried and weighted.

4. Results of the Laboratory Experiment

Different transport regimes governed the two bed reaches. The bimodal reach was dominated by partial transport conditions [*Wilcock and McArdell*, 1993], whereas the sand reach was dominated by fully mobile transport conditions. We first present the results of the sand reach, and subsequently the ones of the bimodal reach. Measured bed elevation changes were related exclusively to the mobility of the sand fraction. The gravel particles were not mobile but did find slightly lower positions due to the washing out of sand.

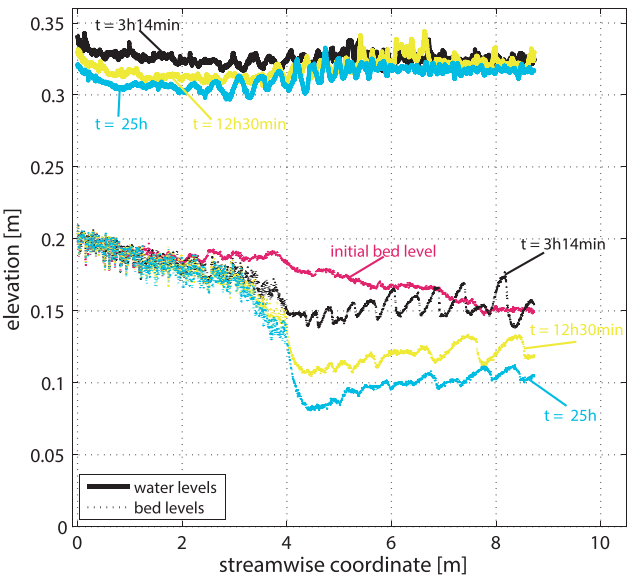

Figure 6. Measured water surface and bed elevation profiles at the initial state, after 3 h 14 min, 12 h 30 min and after 25 h (end of the experiment). Flow is from left to right.

4.1. The Sand Reach

The lack of sediment supply combined with conditions of partial transport resulted in the formation of a static armor over the bimodal reach. The limited amount of sand entrained from the bimodal reach was transported to the sand reach. The sand bed started to degrade since the sediment transport capacity over the sand reach was larger than the sediment supplied from upstream (Figure 6). The sand reach thus started to adjust to a situation without sediment supply and evolved toward a state with a much milder slope and larger flow depth. Degradation primarily occurred in the initial phase of the experiment. Initially, we observed degradation over the upstream part of the sand reach and deposition over the downstream part and subsequently, the degradation wave propagated downstream (Figures 6 and 7b and 7c).

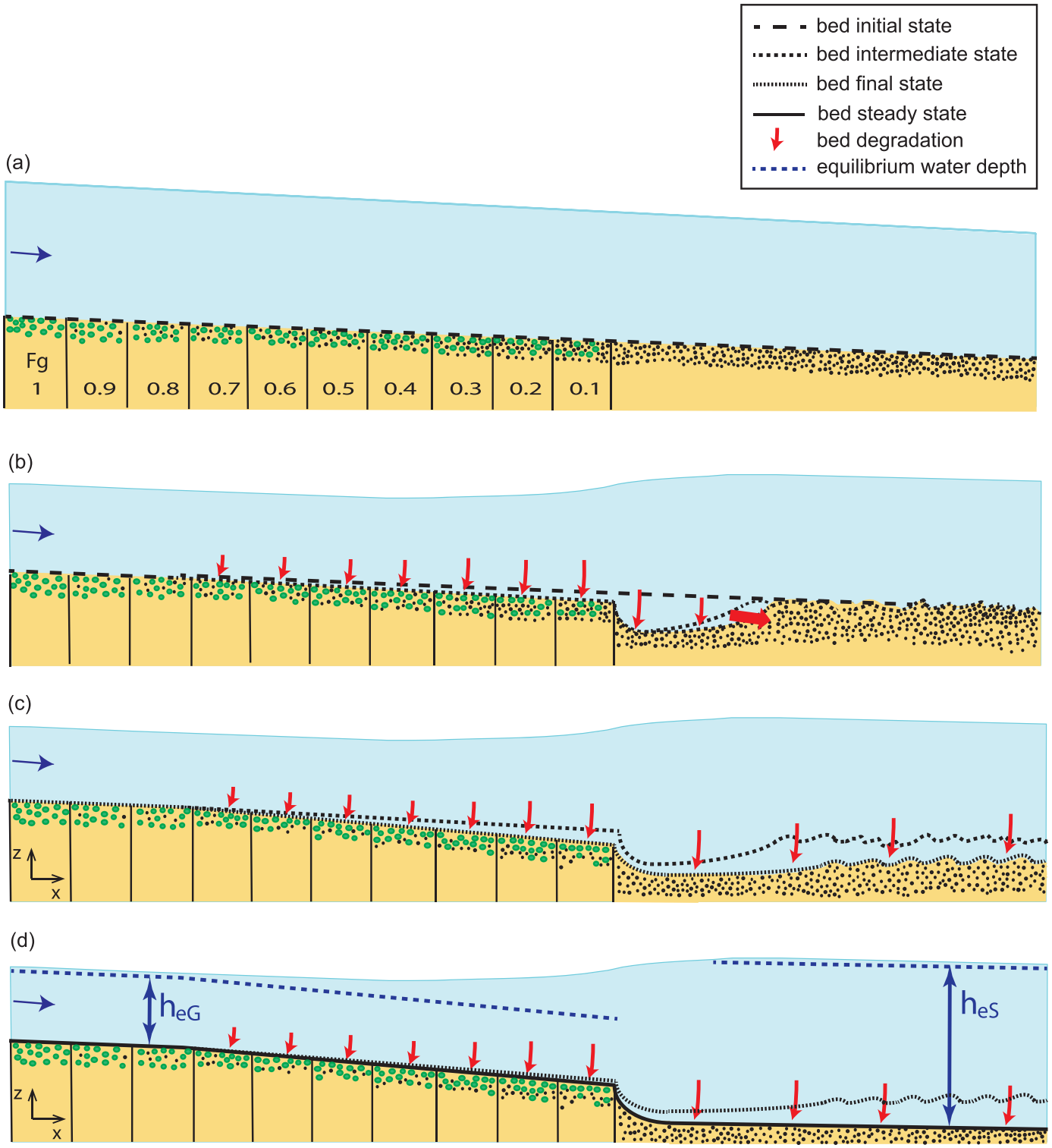

Figure 7. Schematic of the laboratory experiment at the (a) initial state, (b) intermediate state, (c) final state, and (d) hypothetical equilibrium state, in which h_{eG} is the normal flow depth for the bimodal reach, and h_{eS} is the normal flow depth for the sand reach.

The sand reach was dominated by dunes. We observed a temporal decrease of bed form height, indicating the temporal decrease of the sediment transport rate (Figure 6). Relative to a plane bed case in which only skin friction is present, the additional form drag created by the bed forms led to an increased flow depth

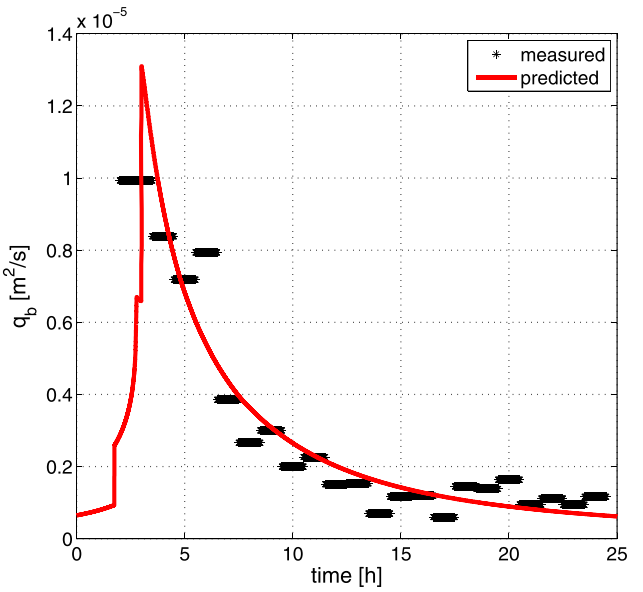

Figure 8. Measured and predicted sediment transport rate at the downstream end of the flume. Please note that for a comparison of predicted and measured data one needs to average predicted data over the same period as each measured data point.

and so an increase of the degradation as the base level was constant. Yet this bed form-related effect decreased with time as bed form height and so form drag decreased with time.

An adverse slope was maintained during the experiment, and the experiment was not completely continued until its equilibrium state was reached. Figure 7c shows a schematic of the final state of the experiment. The equilibrium state in a situation without sediment supply is a state without sediment transport. This was achieved by either a reduction of the slope such that Shields stress is below its critical value (the sand reach) or the washing out of the mobile fractions from a relatively steep reach (the upstream part of the bimodal reach). The approach to a condition of zero transport was also observed in the measured sediment transport rate with time (Figure 8). At the end of the experiment the upstream part of the sand reach was characterized by a plane bed and the downstream part by the presence of dunes. The hypothetical equilibrium state for the sand reach during a state without sediment transport is (close to) a plane bed (Figure 7d).

The above different response between the two reaches to a situation of zero sediment supply (armoring in the bimodal reach versus a strong reduction of the slope in the sand reach) resulted in a spatial decrease in bed elevation between the bimodal and the sand reach (Figure 9) and a relatively sharp expansion of the flow (Figure 6). Such flow expansion results in the so called Bernoulli effect [e.g., *Douglas et al.*, 2005]; in case of a sudden streamwise decrease in bed elevation, conservation of energy yields a streamwise increase in the water surface elevation (Figure 6). The latter was accompanied by a streamwise decrease of the flow velocity and so the sediment mobility.

4.2. The Bimodal Reach

As a result of the difference in bed slope, the normal flow depth for the upstream bimodal reach, h_{eG}, was smaller than the one of the sand reach, h_{eS} (Figure 7d). The subcritical flow conditions and the fact that the normal flow depth was larger than the critical flow depth, led to the presence of an M1 backwater. The M1 backwater resulted in a flow depth larger than the normal one and a streamwise increase of the flow depth over the bimodal reach (Figures 6 and 7), which was accompanied by a streamwise decrease in the Shields stress and sediment mobility. We will consider the consequences of these effects below and in Appendix A.

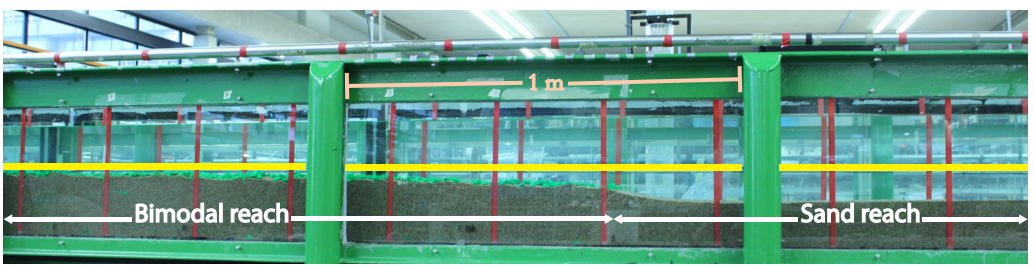

Figure 9. Side view after 16 flow hours of both the bimodal and the sand reach in the central part of the flume. Flow is from left to right. The yellow line indicates the initial bed elevation.

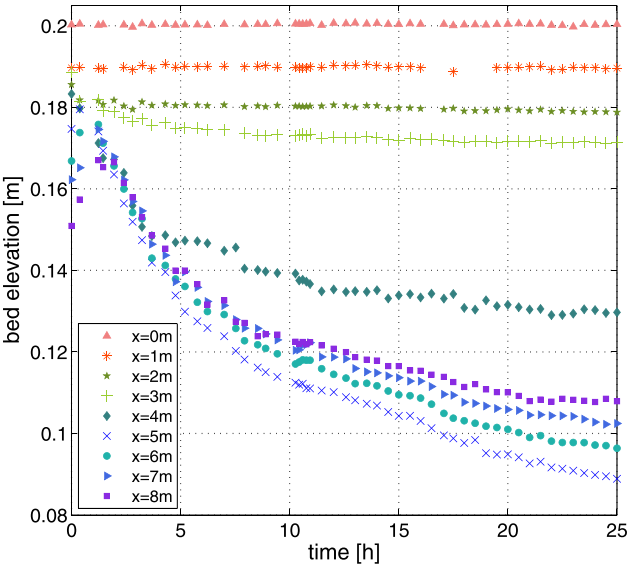

Figure 10. Measured temporal change of the bed elevation at various locations. The measured data have been filtered using a moving average filter to remove the effect of bed forms (compare with Figure 6).

It is worth noting that, had the experiment been continued until its equilibrium state was reached, the M1 backwater would still be present over the bimodal reach (Figure 7d). This is because of the fact that the bimodal reach here acted as a fixed bed, as the gravel was immobile.

The bimodal reach was governed by bed surface coarsening and limited degradation. The streamwise increase in the volume fraction content of sand in the initial bed allowed for the degradation to increase with streamwise position (Figures 6 and 10). The temporal change in bed elevation was therefore limited or negligible over the upstream 3 m of the bimodal reach (Figure 10). Figure 10 shows how at the final state the experiment was approaching its equilibrium state.

As there was no sediment supply and only sand was mobile, the bed surface coarsened and a static armor formed. Such a static armor forms under conditions of relatively low shear stress when the finer grains are mobile while the coarser ones are not [e.g., *Parker and Klingeman*, 1982; *Jain*, 1990]. The armor prevented the underlying finer sediment from being entrained by the flow, limited degradation, and made the initial transition in mean grain size between the two reaches more abrupt (Figure 11). The downstream fining trend over the bimodal reach was persistent, which was due to the M1 backwater effect and the associated streamwise decrease in sand mobility.

The sand reach did not show a temporal change in the bed surface gravel content as the gravel particles were not transported into the sand reach (Figure 12). Just as for the temporal change of bed elevation we observed an initially fast adaptation of the areal fraction content of gravel at the bed surface. The upstream part of the bimodal reach reached its equilibrium state faster than the more downstream part. This is illustrated by comparing the adaptation time scales: the half time of the adaptation of the gravel fraction content at x = 1.3 m was about 2 h and at x=3.8 m it was about 3 h.

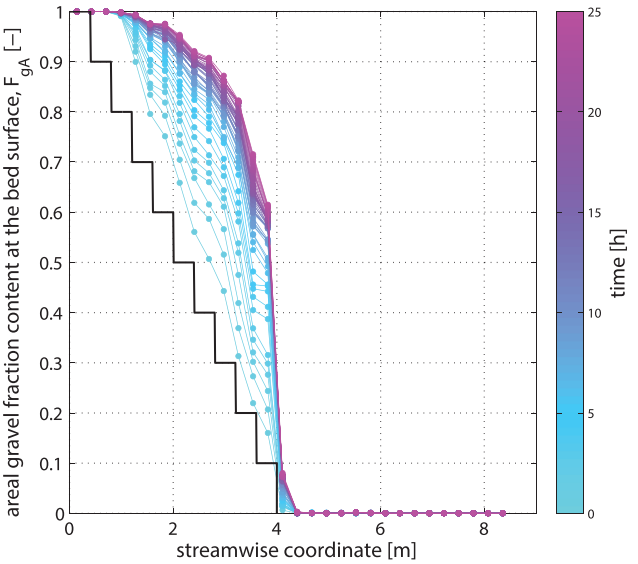

Figure 11. Measured areal gravel fraction content at the bed surface at various times. The imposed initial profile is shown as well (black line).

5. Numerical Model

We apply a one-dimensional model for mixed-sediment morphodynamics to test its capability to reproduce the laboratory experiment. The data on the temporal and spatial evolution of the bed surface resulting from the image analysis technique are used to calibrate the model. The flow submodel accounts for quasi-steady subcritical flow using the backwater equation. The morphodynamic submodel is suitable for sediment mixtures and is based on the active layer approach of *Hirano* [1971]. In this section we will

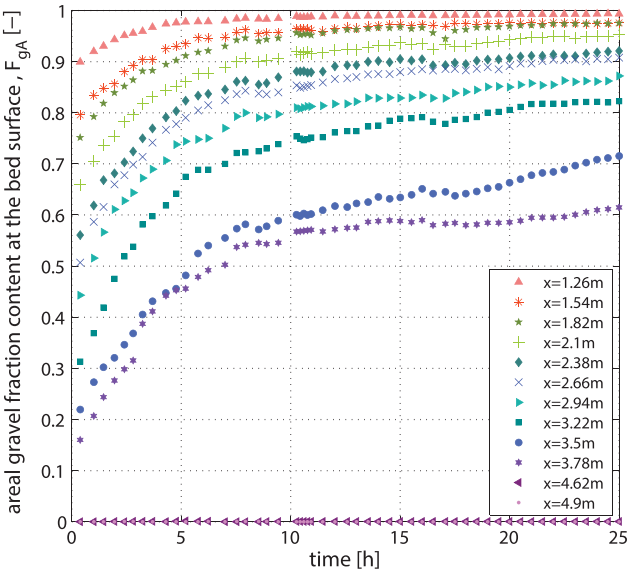

Figure 12. Measured temporal change of the gravel fraction content at the bed surface at various locations.

present the relevant model equations, closure relations, and the model calibration, and in section 6 we will compare predicted results to the measured ones.

5.1. Model Equations

The flow is assumed to be quasi-steady and hence is approximated by the backwater equation, here written in terms of the total energy per unit weight, E, i.e., the total energy head:

$$\frac{\partial E}{\partial x} = -S_f \tag{1}$$

where the friction slope S_f is computed using the relation $S_f = C_{fq} Fr^2$, in which C_{fq} is a nondimensional friction coefficient that accounts for skin friction, form drag, and side wall friction, and Fr is the Froude number. The value of C_{fq} is based on calibration, which is explained in Appendix B. The total energy head E is defined as

$$E = \eta + h + \frac{q^2}{2gh^2} \tag{2}$$

where η is the bed elevation, h is the flow depth, $g = 9.81 m/s^2$ is the acceleration due to gravity, and q is the water discharge per unit width.

The *Hirano* active layer equation describes the temporal change of the volume fraction content of size fraction i at the bed surface, or more precisely in the active layer, and reads [*Hirano*, 1971; *Ribberink*, 1987; *Parker*, 1991a, 1991b]:

$$c_b \frac{\partial F_{ai} L_a}{\partial t} + c_b f_i^l \frac{\partial (\eta - L_a)}{\partial t} + \frac{\partial q_{bi}}{\partial x} = 0 \tag{3}$$

where $c_b = 1 - p$, p being the bed porosity (we assume $p = 0.4$), L_a the active layer thickness, F_{ai} the volume fraction content of size fraction i in the active layer, f_i^l the volume fraction content of size fraction i at the interface between the active layer and the substrate, and q_{bi} is the bedload discharge per unit width of size fraction i. Here subscript i is an index denoting the fine fraction ($i = 1$) or the coarse fraction ($i = 2$). We apply the following definition of the interface fraction content f_i^l:

$$f_i^l = \begin{cases} F_{ai} & \text{if } \partial(\eta - L_a)/\partial t \geq 0 \\ F_{si} & \text{if } \partial(\eta - L_a)/\partial t < 0 \end{cases} \tag{4}$$

where F_{si} denotes the volume fraction content in the substrate just beneath the interface.

If we sum the active layer equations over all size fractions, we retrieve the Exner equation for bed elevation change, which reads:

$$c_b \frac{\partial \eta}{\partial t} + \frac{\partial q_b}{\partial x} = 0 \tag{5}$$

As the sand reach consisted of unisize sediment, the *Hirano* equation and active layer thickness do not play a role. Therefore we can safely define the active layer thickness based on the characteristics of the bimodal reach only, and set the active layer thickness L_a equal to $n_a D_g$. The nondimensional constant n_a is set equal to 1, which is in line with the values proposed by *Parker* [2004] and *Viparelli et al.* [2010] for a plane bed case and D_g is the gravel diameter.

The total bedload discharge per unit width q_b in the Exner equation is given by

$$q_b = q_{b1} + q_{b2} \tag{6}$$

In equations (3) and (6), the grain size specific bedload discharge is computed using the transport relation of Ashida and Michiue [1972]:

$$q_{bi} = 17\sqrt{gRD_i^3}F_{ai}(\tau_i^* - \tau_{ci}^*)(\sqrt{\tau_i^*} - \sqrt{\tau_{ci}^*}) \tag{7}$$

where D_i is the diameter of size fraction i, R is the submerged density ($R = \rho_s/\rho - 1$, in which $\rho_s = 2650\,kg/m^3$ and $\rho = 1000\,kg/m^3$ are the mass density of respectively sediment and water), and τ_{ci}^* is the critical Shields stress of size fraction i. Its value is determined through calibration (Appendix B). Furthermore in equation (7) the Shields stress of size fraction i is defined as $\tau_i^* = C_{fs}q^2/(RD_igh^2)$, where C_{fs} is the friction coefficient related to skin friction, which is smaller than C_{fq} as the latter is the sum of skin friction, form drag, and side wall friction. For the evaluation of the skin friction coefficient, we use the Manning-Strickler relation:

$$C_{fs}^{-1/2} = \alpha_r\left(\frac{h}{k_s}\right)^{1/6} \tag{8}$$

where α_r is a nondimensional constant equal to 8.32, $k_s = n_k D_{sg}$ is the roughness height, where n_k is an empirical parameter in the range $1 \div 3$, here assumed equal to 2.5 [*Cui*, 2007]. D_{sg} is the bed surface geometric mean grain size which is determined from:

$$D_{sg} = D_{ref}2^{-\phi_m} \tag{9}$$

$$\phi_m = F_{a1}\phi_1 + F_{a2}\phi_2 \tag{10}$$

$$\phi_i = -log_2\left(\frac{D_i}{D_{ref}}\right) \tag{11}$$

where D_{ref} denotes the reference grain size ($D_{ref} = 1$ mm), ϕ_i the grain size on ϕ-scale of size fraction i, and ϕ_m is the geometric mean grain size on ϕ-scale. Finally in equation (7), the critical Shields stress of the size fraction i is defined as

$$\tau_{ci}^* = \xi_i\tau_{scg}^* \tag{12}$$

where τ_{scg}^* is the critical Shields stress of unisize sediment and ξ_i is the hiding coefficient computed following *Viparelli et al*. [2010]:

$$\xi_i = \begin{cases} \left(\frac{D_i}{D_{sg}}\right)^{-m} & \text{for } \dfrac{D_i}{D_{sg}} \le 1 \\ \left(\frac{D_i}{D_{sg}}\right)^{-n} & \text{for } \dfrac{D_i}{D_{sg}} > 1 \end{cases} \tag{13}$$

where m and n are constants between 0 and 1. Hiding effects are due to the fact that grains of different size at the bed surface experience a different exposure to the flow. Fine grains find shelter in the lee of coarser grains, thus becoming less mobile than under unisize conditions. In turn, coarse grains are more exposed to the flow than under unisize conditions and become more mobile [e.g., *Einstein*, 1950]. As such, hiding effects reduce the grain-size selectivity of the transport process. In equation (13) hiding is negligible if $m = 0$, and equal mobility is achieved if $m = 1$ [*Viparelli et al*., 2010]. The value of m is determined through calibration (Appendix B). The exponent n is set equal to m. The role of n is limited here as the gravel is immobile.

In Appendix B we describe the details of applying the numerical model to our laboratory experiment. In the next section we will compare the predicted results to the measured ones.

6. Comparison Between Measured and Predicted Data

The predicted and measured water surface elevation, bed elevation, and volumetric gravel fraction at the bed surface are compared in Figure 13. We observe similar trends of the predicted and measured bed

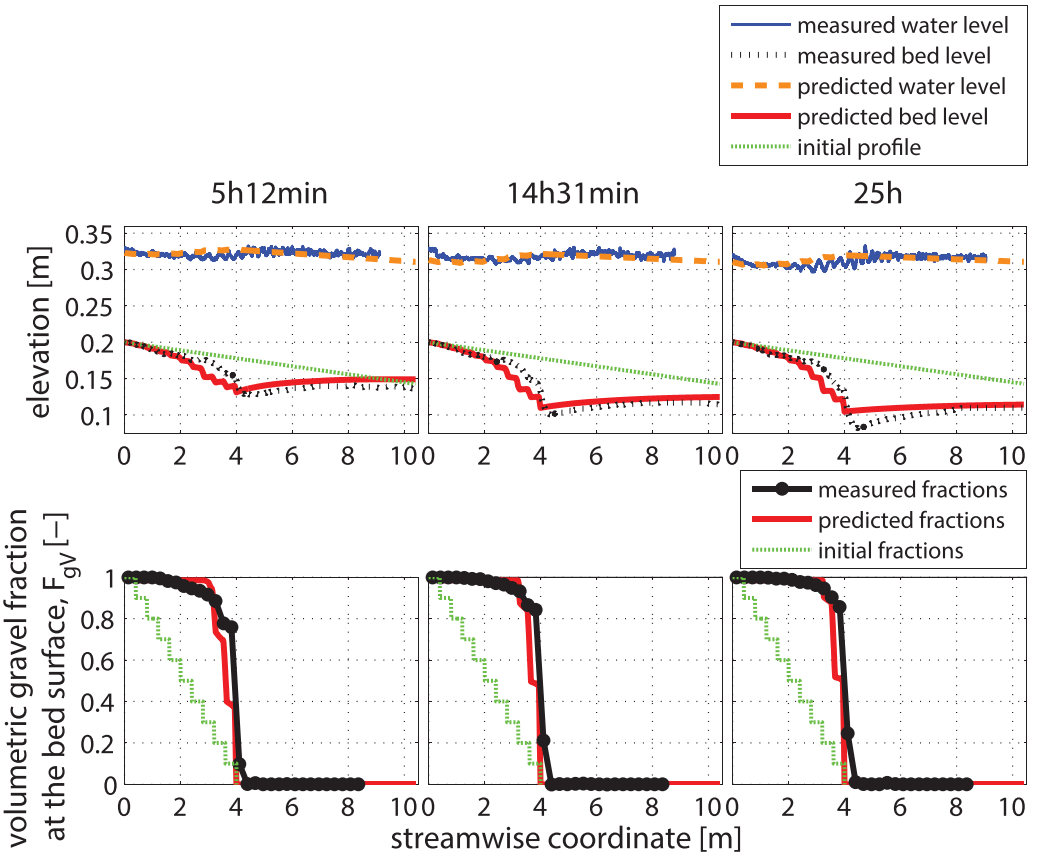

Figure 13. Comparison of measured and predicted water surface elevation and bed elevation and volumetric gravel fraction at the bed surface after 5 h12 min, 14 h 31 min and 25 h.

elevation changes, and the temporal changes are larger in the first 5 h of the experiment. In the downstream part of the bimodal reach, the model slightly overestimates the amount of bed degradation. In the experiment the washing out of sand from the immobile gravel bed may have resulted in a temporal increase of the gravel bed porosity over the bimodal reach. Such temporal change of the bed porosity cannot be represented by the current version of our code. A slight underprediction of the bed level is found in the upstream part of the sand reach at the end of the simulation.

Measured and predicted sediment transport rates at the downstream end of the flume are compared in Figure 8. Please note that for a comparison of predicted and measured data, one needs to average predicted data over the same period as each measured data point. The sediment transport relation of *Ashida and Michiue* [1972] appears to well capture the different sediment transport regimes dominating the bimodal reach and the sand reach. In particular, partial transport is represented well as the predicted gravel Shields stress never exceeds its critical value. The model predicts the temporal decreasing trend of the sediment transport rate well, with a slight underestimation in the final part of the experiment. This underestimation is in line with the slightly underpredicted degradation over the sand reach (bed elevation at $t = 25h$ in Figure 13).

The final state of the grain size distribution of the bimodal reach is reproduced fairly well by the numerical model (Figure14). Yet the coarsening process predicted by the model was somewhat too slow. In the experiment the sand entrainment quickly led to a coarse bed surface (Figure 14), whereas the time scale of coarsening in the model is larger. This may be associated with the aforementioned temporal increase of the porosity of the surface layer. In the model the entrainment of sand leads to degradation and lowering of the active layer without a temporal change of the porosity, which results in entrainment of finer substrate sediment into the active layer. In the model this sand then becomes available for entrainment by the flow, which may be the reason of the slight overprediction of the bed degradation in the bimodal reach.

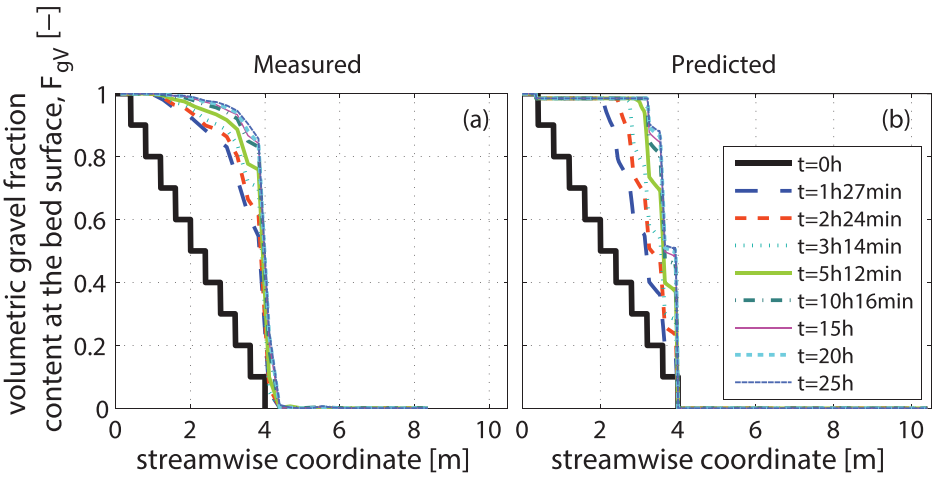

Figure 14. Comparison between (a) measured and (b) predicted volumetric gravel fraction content at the bed surface.

7. Discussion

Although many laboratory experiments have focused on armoring processes [*Little and Mayer*, 1972; *Church et al*., 1998; *Hassan and Church*, 2000; *Hassan et al*., 2006], a relevant feature of the static armor considered here is the fact that it is governed by downstream fining, resulting from the presence of the M1 backwater and the associated streamwise reduction in sand mobility. Here downstream fining is the result of an erosional process and not due to depositional processes as studied in other laboratory experiments [*Paola et al*., 1992; *Seal et al*., 1997; *Toro-Escobar et al*., 2000].

Similar to the laboratory experiments of *Paola et al*. [1992] and *Seal et al*. [1997], we observed a sharp transition from a gravel to a sand reach, which is associated with a break in slope. An abrupt transition in slope and bed surface grain size between a gravel bed reach and a sand bed reach is observed in many rivers and is termed a gravel-sand transition [e.g., *Yatsu*, 1955; *Shaw and Kellerhals*, 1982; *Parker*, 1991a, 1991b; *Frings*, 2011; *Venditti et al*., 2015]. Although our findings suggest a similarity between the experiment and a natural gravel-sand transition, our case is governed by an initial bed that was characterized by a stepwise fining pattern and only two fractions, a lack of sediment supply, and a restriction to periods of base flow in which the coarse material is immobile. Moreover, we have excluded many aspects that have been recognized to be relevant to the development of a gravel-sand transition such as the progradation of a gravel wedge [*Paola et al*., 1992; *Seal et al*., 1997], basin subsidence [*Paola*, 1988; *Parker and Cui*, 1998], base level change [*Pickup and Warner*, 1984; *Sambrook Smith and Ferguson*, 1995], abrasion [*Yatsu*, 1955; *Parker and Cui*, 1998] and suspended load [*Venditti and Church*, 2014; *Venditti et al*., 2015]. We are therefore hesitant to claim a similarity between the mechanisms in our experiment and a gravel-sand transition in the field.

Although not measured, we expect that in our experiment the bed porosity varied spatially and temporally. Also the bed structure, i.e., a clast-supported or a matrix-supported bed [*Carling and Reader*, 1982; *Wilcock*, 1998], may have varied spatially and temporally. The upstream part of the bimodal reach was likely clast-supported. Further downstream in the bimodal reach where the sand content was larger than 20–40%, we expect the bed structure to be matrix supported [*Wilcock*, 1998]. Although not measured, the experiment may have resulted in a change of the bed structure in the downstream part of the bimodal reach from a matrix-supported to a clast-supported one. In such a situation sand constitutes the pore-filling load that can be entrained from the pores resulting in porosity changes limiting morphodynamic change [e.g., *Frings et al*., 2008]. The current version of the morphodynamic model is not capable of reproducing such temporal changes in bed porosity.

8. Conclusions

We present a new image analysis technique that is suitable for estimating spatial and temporal changes in the grain size distribution of the bed surface during flow in a laboratory experiment. Different from a

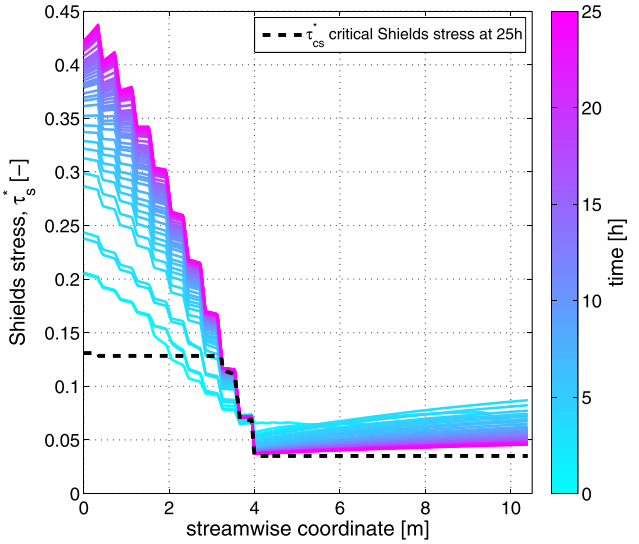

Figure 15. Shields stress for the sand fraction predicted by the numerical model at various times. The dashed black line indicates the sand-related critical Shields stress at the end of the simulation.

previous method [*Orrú et al.*, 2014], the technique can be used during flow with transported sediment. Also, the new algorithm provides an improved color segmentation of shadow-rich grains, allows for 6 well-sorted grain size fractions, and allows for using color combinations in which one of the sediment fractions (sand) is unpainted to avoid cohesion-related problems.

The new image analysis technique was applied to a degradational sand-gravel laboratory experiment. Conditions of partial transport and limited sediment supply resulted in the formation of a static armor over the upstream bimodal reach. The initially gradual streamwise transition in grain size resulted in a more abrupt transition in grain size between the upstream sand-gravel reach and the downstream sand reach. The static armor was characterized by downstream fining due to an M1 backwater that induced a decrease in sand mobility toward the transitional point.

Although under steady flow a morphodynamic equilibrium state is generally expected to be governed by normal flow, the equilibrium state of the examined case is governed by the presence of a backwater, as gravel immobility (partial transport) prevented the bimodal reach from establishing normal flow conditions.

The detailed measurements of the temporal and spatial changes of bed surface texture enabled an improved calibration of the numerical model and in particular the calibration of the hiding coefficient in the sediment transport relation. The numerical mixed-sediment model captured the hydrodynamic and the morphodynamic adjustment to the shortage of sediment supply and the coarsening of the bed surface, except for the time scale of the coarsening process.

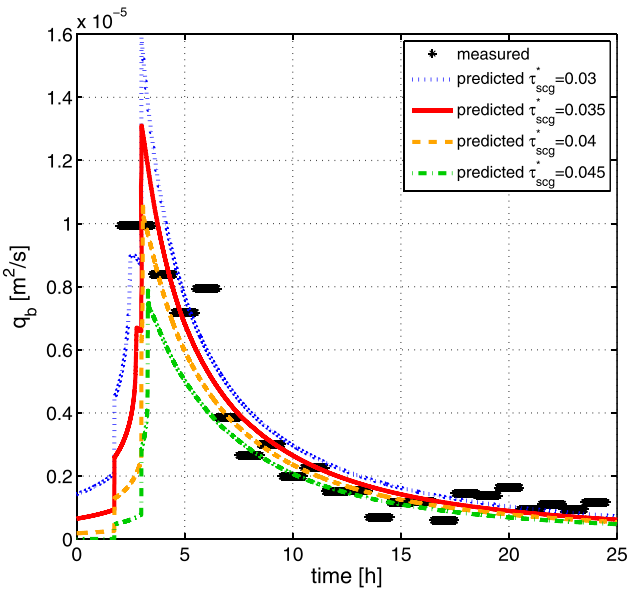

Figure 16. Comparison of the measured and predicted sediment transport rate at the downstream end of the flume for different values of critical Shields stress. Please note that for a comparison of predicted and measured data one needs to average predicted data over the same period as each measured data point.

Appendix A: Backwater Effect Over the Bimodal Reach

The presence of an M1 backwater affected the sediment mobility over the bimodal reach. As mentioned in section 4.2, the streamwise increase of the flow depth over the bimodal reach led to a streamwise decrease of the sediment mobility. In order to assess this effect we have evaluated the mobility of the sand fraction. Figure 15 shows the predicted values of the Shields stress of the sand fraction. The spatial gradient of the sand mobility over the bimodal reach increases with time due to the presence of the backwater. In particular, in the upstream part of the bimodal reach we

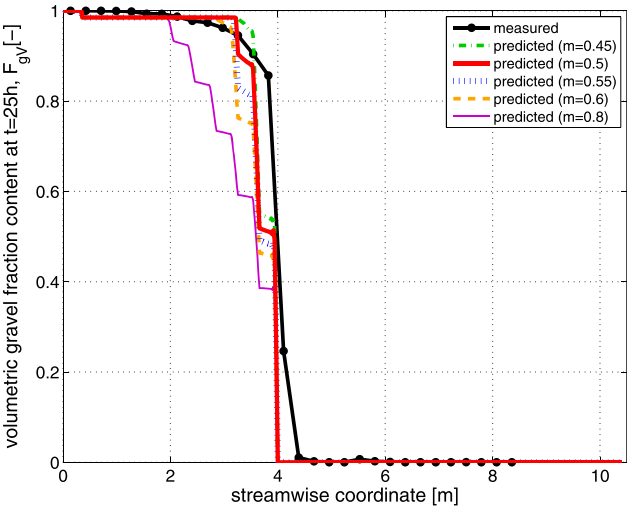

Figure 17. Comparison of the measured and predicted volumetric gravel fraction content at the bed surface at 25 flow hours for different values of the hiding exponent *m*.

observe a large temporal increase of the Shields stress due to the decrease of the water surface elevation. The downstream part of the bimodal reach shows a smaller temporal increase of the sand mobility. The difference between the upstream and the downstream part of the bimodal reach illustrates the increase of the backwater effect during the experiment. The evolution toward the equilibrium state of the sand reach can be observed in Figure 15 as it is slowly approaching conditions of zero transport.

Appendix B: Model Application

In this section we describe the application of the numerical model to the laboratory experiment and, in particular, the steps undertaken to calibrate the numerical model. The initial and boundary conditions for the simulation were equal to the ones imposed in the experiment (section 3.1). The upstream boundary conditions were the water and sediment discharge and the downstream one was the base level. The measured areal fraction content of the size fractions at the bed surface provided by the image analysis technique were converted, as explained in *Orrú et al.* [2014], into a volumetric fraction content using the conversion model of *Parker* [1991a, 1991b]. The numerical model does not explicitly deal with individual bed forms as it predicts bed form-averaged behavior, and measured bed form-averaged bed elevation data were found using a moving average filter.

The parameters used to calibrate the model were (a) the hydraulic friction coefficient, C_{fq}, introduced just below equation (1), (b) the critical Shields stress, τ^*_{scg}, in equation (12), and (c) the exponent of the hiding coefficient, *m*, in equation (13). The model calibration was subdivided into two steps: the hydrodynamic and the morphodynamic calibration. The value of the hydraulic friction coefficient C_{fq} was estimated predicting the flow based on the measured bed elevation profiles at all times. The parameter was optimized comparing the outcome of measured and predicted water surface elevation, and its optimal value was found to be 0.011.

In the morphodynamic calibration the critical Shields stress τ^*_{scg} and the exponent of the hiding coefficient *m* were calibrated jointly. For the critical Shields stress τ^*_{scg} we studied the influence of the threshold of motion comparing the measured and predicted data of the sediment transport rate at the downstream end, as well as the temporal changes of the bed elevation and volumetric gravel fraction content at the bed surface. Predicted results for a critical Shields stress equal to $\tau^*_{scg}=0.035$ well compare to the measured ones (Figure 16). Further, we assessed the predicted results for different values of the exponent *m* in the hiding coefficient (equation (13)). An increase in *m* reflects a reduction of the sand mobility. To optimize the value of *m* we examined the bed surface volumetric gravel fraction content and bed elevation for different values of the exponent *m* (Figure 17). Optimal results were found for *m* equal to 0.5. This value is in line with the range proposed by *Frings* [2008] who suggests values between $0.3 < m < 0.7$ for strongly bimodal sediment mixtures.

Acknowledgments
The contributions of Orrú, Chavarrías, and Stecca were funded through Aspasia scholarship 015.007.051 awarded to Blom by the Netherlands Organization for Scientific Research (NWO) and scholarship 10.015 of the Dr ir Cornelis Lely Stichting. Ferrara was funded through a Training Agreement in the LLP/ERASMUS Programme. Stecca is currently funded by a Marie Curie International Outgoing Fellowship (project BraidSideEarth, grant 2013-621886). The data used in the analysis can be found at the link https://surfdrive.surf.nl/files/public.php?service=files&t=9cea09540608b0da5d8bc53f14f456d4.

References

Alves, E., and A. Cardoso (1999), Experimental study on aggradation, *Int. J. Sediment Res.*, *14*(1), 1–15.
Ashida, K., and M. Michiue (1972), Study on hydraulic resistance and bedload transport rate in alluvial streams, *Trans. Jpn. Soc. Civ. Eng.*, *206*, 56–69.
Bhamidipaty, S., and H. W. Shen (1971), Laboratory study of degradation and aggradation, *J. Waterw. Harbors Coastal Eng. Div. Am. Soc. Civ. Eng.*, *97*(4), 615–630.
Blom, A., J. S. Ribberink, and H. J. de Vriend (2003), Vertical sorting in bed forms: Flume experiments with a natural and a trimodal sediment mixture, *Water Resour. Res.*, *39*(2), 1025, doi:10.1029/2001WR001088.
Carling, P. A., and N. A. Reader (1982), Structure, composition and bulk properties of upland stream gravels, *Earth Surf. Processes Landforms*, *7*(4), 349–365, doi:10.1002/esp.3290070407.

Church, M., M. A. Hassan, and J. F. Wolcott (1998), Stabilizing self-organized structures in gravel-bed stream channels: Field and experimental observations, *Water Resour. Res.*, *34*(11), 3169–3179, doi:10.1029/98WR00484.
Crowe Curran, J., and K. A. Waters (2014), The importance of bed sediment sand content for the structure of a static armor layer in a gravel bed river, *J. Geophys. Res. Earth Surf.*, *119*, 1484–1497, doi:10.1002/2014JF003143.
Cui, Y. (2007), The unified gravel-sand (TUGS) model: Simulating sediment transport and gravel/sand grain size distributions in gravel-bedded rivers, *Water Resour. Res.*, *43*, W10436, doi:10.1029/2006WR005330.
Douglas, J., J. Gasiorek, J. Swaffield, and L. Jack (2005), *Fluid Mechanics*, 5th ed., Pearson Prentice Hall, Harlow.
Einstein, H. A. (1950), *The Bed-Load Function for Sediment Transportation in Open Channel Flows*, 1026 pp., US Dep. of Agric., Washington, D. C.
Frings, R. M. (2008), Downstream fining in large sand-bed rivers, *Earth Sci. Rev.*, *87*(12), 39–60, doi:10.1016/j.earscirev.2007.10.001.
Frings, R. M. (2011), Sedimentary characteristics of the gravel–sand transition in the River Rhine, *J. Sediment. Res.*, *81*(1), 52–63.
Frings, R. M., M. G. Kleinhans, and S. Vollmer (2008), Discriminating between pore-filling load and bed-structure load: A new porosity-based method, exemplified for the river Rhine, *Sedimentology*, *55*(6), 1571–1593, doi:10.1111/j.1365-3091.2008.00958.x.
Galay, V. J. (1983), Causes of river bed degradation, *Water Resour. Res.*, *19*(5), 1057–1090, doi:10.1029/WR019i005p01057.
Gölz, E. (1994), Bed degradation–Nature, causes, countermeasures, *Water Sci. Technol.*, *29*(3), 325–333.
Hassan, M. A., and M. Church (2000), Experiments on surface structure and partial sediment transport on a gravel bed, *Water Resour. Res.*, *36*(7), 1885–1895, doi:10.1029/2000WR900055.
Hassan, M. A., R. Egozi, and G. Parker (2006), Experiments on the effect of hydrograph characteristics on vertical grain sorting in gravel bed rivers, *Water Resour. Res.*, *42*, W09408, doi:10.1029/2005WR004707.
Heays, K. G., H. Friedrich, and B. W. Melville (2010a), Re-evaluation of image analysis for sedimentary process research, *Proceedings of IAHR APD Congress*, International Association for Hydro-Environment Engineering and Research, Asia Pacific Division, Auckland.
Heays, K. G., H. Friedrich, and B. W. Melville (2010b), Advanced particle tracking for sediment movement on river beds: A laboratory study, in *17th Australasian Fluid Mechanics Conference, Univ. of Auckland, Auckland, New Zealand*, pp. 5–9.
Heays, K. G., H. Friedrich, and B. W. Melville (2014), Laboratory study of gravel-bed cluster formation and disintegration, *Water Resour. Res.*, *50*, 2227–2241, doi:10.1002/2013WR014208.
Hirano, M. (1971), River bed degradation with armouring, *Trans. Jpn. Soc. Civ. Eng.*, *3*(195), 55–65.
Jain, S. (1990), Armor or pavement, *J. Hydraul. Eng.*, *116*(3), 436–440, doi:10.1061/(ASCE)0733-9429(1990)116:3(436).
Little, W., and P. Mayer (1972), *The Role of Sediment Gradation on Channel Armoring*, Environ. Resour. Cent., Georgia Inst. of Technol., Atlanta.
Mao, L., J. R. Cooper, and L. E. Frostick (2011), Grain size and topographical differences between static and mobile armour layers, *Earth Surf. Processes Landforms*, *36*(10), 1321–1334, doi:10.1002/esp.2156.
Newton, C. T. (1951), An experimental investigation of bed degradation in an open channel, *Trans. Boston Soc. Civ. Eng.*, *195*, 28–60.
Orrú, C., V. Chavarrías, W. S. J. Uijttewaal, and A. Blom (2014), Image analysis for measuring the size stratification in sand-gravel laboratory experiments, *Earth Surf. Dyn.*, *2*(1), 217–232, doi:10.5194/esurf-2-217-2014.
Paola, C. (1988), Subsidence and gravel transport in alluvial basins, in *New Perspectives in Basin Analysis*, edited by K. L. Kleinspehn, and C. Paola, pp. 231–243, Springer, N. Y.
Paola, C., G. Parker, R. Seal, S. K. Sinha, J. B. Southard, and P. R. Wilcock (1992), Downstream fining by selective deposition in a laboratory flume, *Science*, *258*(5089), 1757–1760, doi:10.1126/science.258.5089.1757.
Parker, G. (1991a), Selective sorting and abrasion of river gravel I: Theory, *J. Hydraul. Eng.*, *117*(2), 131–147, doi:10.1061/(ASCE)0733-9429(1991)117:2(131).
Parker, G. (1991b), Selective sorting and abrasion of river gravel II: Applications, *J. Hydraul. Eng.*, *117*(2), 150–171, doi:10.1061/(ASCE)0733-9429(1991)117:2(150).
Parker, G. (2004), *1D sediment Transport Morphodynamics With Applications to Rivers and Turbidity Currents*, University of Illinois. [Available at http://vtchl.uiuc.edu/people/parkerg/morphodynamics e-book.htm.]
Parker, G., and Y. Cui (1998), The arrested gravel front: Stable gravel-sand transitions in rivers part 1: Simplified analytical solution, *J. Hydraul. Res.*, *36*(1), 75–100, doi:10.1080/00221689809498379.
Parker, G., and P. Klingeman (1982), On why gravel bed streams are paved, *Water Resour. Res.*, *18*(5), 1409–1423, doi:10.1029/WR018i005p01409.
Pickup, G., and R. Warner (1984), Geomorphology of tropical rivers II. Channel adjustment to sediment load and discharge in the Fly and lower Purari, Papua New Guinea, *Catena*, *5*, 18–41.
Piedra, M. M., H. Haynes, and T. B. Hoey (2012), The spatial distribution of coarse surface grains and the stability of gravel river beds, *Sedimentology*, *59*(3), 1014–1029, doi:10.1111/j.1365-3091.2011.01290.x.
Ribberink, J. S. (1987), Mathematical modelling of one-dimensional morphological changes in rivers with non-uniform sediment, PhD thesis, Delft Univ. of Technol., Delft, Netherlands.
Sambrook Smith, G. H., and R. I. Ferguson (1995), The gravel-sand transition along river channels, *J. Sediment. Res.*, Sect. A, *65*(2), 423–430.
Seal, R., C. Paola, G. Parker, J. Southard, and P. R. Wilcock (1997), Experiments on downstream fining of gravel I: Narrow-channel runs, *J. Hydraul. Eng.*, *123*(10), 874–884, doi:10.1061/(ASCE)0733-9429(1997)123:10(874).
Shaw, J., and R. Kellerhals (1982), *The Composition of Recent Alluvial Gravels in Alberta River Beds*, Bulletin Alberta Research Council 41, Alberta Geol. Surv. and Alberta Res. Counc., Alberta.
Soni, J. (1981), Laboratory study of aggradation in alluvial channels, *J. Hydrol.*, *49*(12), 87–106, doi:10.1016/0022-1694(81)90207-9.
Suzuki, K., and M. Michue (1991), Propagation and deformation of a low mound formed on a river bed and sorting of bed surface mixtures, paper presented at 24th IAHR Congress, Madrid.
Toro-Escobar, C., C. Paola, G. Parker, P. Wilcock, and J. Southard (2000), Experiments on downstream fining of gravel II: Wide and sandy runs, *J. Hydraul. Eng.*, *126*(3), 198–208, doi:10.1061/(ASCE)0733-9429(2000)126:3(198).
Venditti, J. G., and M. Church (2014), Morphology and controls on the position of a gravel-sand transition: Fraser river, British Columbia, *J. Geophys. Res. Earth Surf.*, *119*, 1959–1976, doi:10.1002/2014JF003147.
Venditti, J. G., N. Domarad, M. Church, and C. D. Rennie (2015), The gravel-sand transition: Sediment dynamics in a diffuse extension, *J. Geophys. Res. Earth Surf.*, *120*, 943–963, doi:10.1002/2014JF003328.
Viparelli, E., O. E. Sequeiros, A. Cantelli, P. R. Wilcock, and G. Parker (2010), River morphodynamics with creation/consumption of grain size stratigraphy II: Numerical model, *J. Hydraul. Res.*, *48*(6), 727–741, doi:10.1080/00221686.2010.526759.
Wilcock, P. R. (1998), Two-fraction model of initial sediment motion in gravel-bed rivers, *Science*, *280*(5362), 410–412, doi:10.1126/science.280.5362.410.
Wilcock, P. R., and B. W. McArdell (1993), Surface-based fractional transport rates: Mobilization thresholds and partial transport of a sand-gravel sediment, *Water Resour. Res.*, *29*(4), 1297–1312, doi:10.1029/92WR02748.

Wilcock, P. R., S. T. Kenworthy, and J. C. Crowe (2001), Experimental study of the transport of mixed sand and gravel, *Water Resour. Res.*, *37*(12), 3349–3358, doi:10.1029/2001WR000683.

Wu, F., and K. Yang (2004), A stochastic partial transport model for mixed-size sediment: Application to assessment of fractional mobility, *Water Resour. Res.*, *40*, W04501, doi:10.1029/2003WR002256.

Yatsu, E. (1955), On the longitudinal profile of the graded river, *Eos Trans. AGU*, *36*(4), 655–663, doi:10.1029/TR036i004p00655.

Yen, C., S. Chang, and H. Lee (1992), Aggradation and degradation process in alluvial channels, *J. Hydraul. Eng.*, *118*(12), 1651–1669, doi: 10.1061/(ASCE)0733-9429(1992)118:12(1651).